AIAA 97-0567

Overview of X-38 Hypersonic Wind Tunnel Data and Comparison with Numerical Results

C. Campbell and J. Caram
NASA Johnson Space Center
Houston, TX

S. Berry, M. DiFulvio and T. Horvath
NASA Langley Research Center
Hampton, VA

35th Aerospace Sciences Meeting & Exhibit
January 6-10, 1997 / Reno, NV

An Overview of X-38 Hypersonic Wind Tunnel Data and Comparison with Numerical Results

Charles H. Campbell*
Jose Caram*
NASA Johnson Space Center
Houston, TX

Scott Berry,** Michael DiFulvio** and Tom Horvath**
NASA Langley Research Center
Hampton, VA

Abstract

A NASA team of engineers has been organized to design a crew return vehicle for returning International Space Station crew members from orbit. The hypersonic characteristics of this X-23/X-24A derived crew return vehicle (designated X-38) are being evaluated in various wind tunnels in support of this effort. Aerodynamic data has been acquired in three NASA hypersonic facilities at Mach 20, and Mach 6. Computational Fluid Dynamics tools have been applied at the appropriate wind tunnel conditions to make comparisons with portions of this data. Experimental data from the Mach 6 Air and CF4 facilities illustrate a net positive pitching moment increment due to density ratio, as well as increased elevon effectiveness. Chemical nonequilibrium computational fluid dynamics solutions at flight conditions reinforce this conclusion.

Nomenclature

b	=	reference wingspan, in.	c	=	reference chord, in.
L	=	X-38 reference length, in.	S_{ref}	=	reference area, in^2
Xref	=	X aerodynamic reference	Z_{ref}	=	Z aerodynamic reference
M_∞	=	freestream Mach number	P_t	=	stagnation pressure, psia
T_t	=	stagnation temperature, °F	γ_2	=	normal shock ratio of specific heats
q_∞	=	free stream dynamic pressure			
ρ_∞/ρ_2	=	normal shock density ratio	α	=	angle of attack, deg.
C_A	=	axial force/$q_\infty S_{ref}$	C_l	=	roll moment/$q_\infty S_{ref} b$
C_N	=	normal force/$q_\infty S_{ref}$	C_m	=	pitch moment/$q_\infty S_{ref} b$
C_Y	=	side force/$q_\infty S_{ref}$	C_n	=	yaw moment/$q_\infty S_{ref} b$
Re_∞	=	freestream unit Reynolds number, ft^{-1}			
$Re_{\infty,L}$	=	Reynolds number based on reference length			

* Aerospace Engineer, Aerosciences Branch, NASA Johnson Space Center, Member AIAA
** Aerospace Engineer, Aerothermodynamics Branch, NASA Langley Research Center, Member AIAA

Introduction

A NASA Johnson Space Center team of engineers has been organized to design a crew return vehicle (X-38) for returning six International Space Station (ISS) crew members to Earth based on the X-23/X-24A lifting body configuration (see Figure 1). Lifting bodies are extremely beneficial for this type of mission because their good aerodynamic performance provides increased cross range capability which ultimately leads to a shorter on-orbit loiter time. The X-23/X-24A configurations have flown (circa 1965-1967) in the hypersonic/supersonic regime during the United States Air Force sponsored sub-orbital flights of the X-23 (PRIME) and the transonic/runway landings of the X-24A (PILOT) programs. The aerodynamic and aerothermodynamic heating information recovered from the X-23 and X-24A programs have served as the basis for preliminary trajectory and aerothermodynamic environment definitions[1-2]. However, because the X-38 design is a hybrid of these two configurations in order to fly hypersonically as well as subsonically, the aerodynamic and aerothermodynamic databases are being redeveloped with modern wind tunnel and numerical techniques. This includes examining the effects of specific heat ratio upon the hypersonic aerodynamics. Testing in the Mach 6 CF4 facility at LaRC simulates the higher density and lower specific heat ratios characteristic of the high mach number flight environment.

Experimental Methods

Models

The 0.021 scale models used for this study made use of standard metal model fabrication techniques, as well as rapid prototyping using a stereo lithography system. See Table I for X-38 reference dimensions. The model for the Mach 20 He study made use of a single fuselage, removable left and right elevons, and a removable upper ramp corresponding to the upper elevon. This model was generated entirely with the stereo lithography technique. The metal model for the Mach 6 studies was made of numerically machined aluminum and steel, depending on the component involved. The fuselage was manufactured in two pieces; a forebody and the remainder of the fuselage minus the fins. The fins were manufactured separately and attached to the fuselage prior to testing. The outer mold line of the metal model was validated against the CAD definition of the X-38 and the windward side was found to be accurate within 0.005 inches. Like the Mach 20 He model, the left and right elevons were manufactured as wedges that attached onto the fuselage, and the upper ramp was also removable. To ensure maximum model size without serious risk of tunnel blockage, the models were both manufactured to a scale of 0.021. Elevons were manufactured for 15°-30° deflections in 5° increments. In order to accommodate a sting insert, both models had a cylindrical protrusion on the aft upper surface. Maintaining the windward surface was deemed critical for acquiring proper hypersonic aerodynamic results in the primary angle of attack range above 15°. The effect of the leeside protrusion on the integrated aerodynamics was deemed within the measurement accuracy because the leeside flow becomes separated and the surface shadowed above 15°.

Facilities

Three conventional blow down hypersonic wind tunnels will be used in this study. They are the NASA LaRC 20-Inch Mach 6 Air Tunnel, 20-Inch Mach 6 CF4 Tunnel, and the 22-Inch Mach 20 Helium Tunnel. The major components of each are a high pressure bottlefield, settling chamber, nozzle, test section, diffuser, and vacuum spheres. The flow is heated by an electrical resistance heater in the 20-Inch Mach 6 Air Tunnel. The helium facility has the capability to heat the flow but it is not necessary to avoid liquefaction, and the CF4 facility uses a salt bath heater. All tunnels have an injection system which can insert models from a sheltered position to the tunnel centerline in approximately 0.5 seconds. Flow conditions, i.e. Mach number, are determined from

calibrations using measured reservoir values as inputs for the Helium facility, and from the ratio of a measured pitot probe pressure to stagnation pressure to obtain Mach number for the Mach 6 facilities. More detailed descriptions, nominal flow conditions, and recent calibrations are available elsewhere[3-4].

Testing Techniques

Aerodynamics and Flow Visualization: Aerodynamic data has been obtained using a six-component force-and-moment balance for an α range of 0° to 50°. In all cases, the water cooled balance was attached to a straight sting and mounted to the model through the base. A run is conducted by establishing flow in the test section, injecting the model, and then moving through an angle of attack range in a pitch pause manner. The model is then retracted and the tunnel shut down. Free stream conditions were selected to facilitate the use of a single balance in all three facilities, and to eliminate the potential uncertainty associated with the use of different balance hardware. A water cooled balance was selected to provide accurate data over the anticipated load range and minimize errors associated with balance heating. Time histories of the data are typically recorded during an individual run and then averaged over a one second interval at the desired angles of attack. Schleiren photographs were taken as needed to resolve shock structures in the Mach 6 facilities, and surface oil flows were obtained in the Mach 6 air tunnel to better understand the boundary layer behavior on the windward surface.

Test Conditions and Data Reduction: Typical flow conditions for the three tunnels utilized are listed in Table II. Base pressure measured at one or two locations during each run can be used to correct the data to freestream pressure on the base. These corrections have not been applied to the present data sets. Results in the Mach 20 Helium facility were obtained at a $Re_{\infty,L}$ of $3x10^6$ for α between 20° and 50°. Mach 6 air results were obtained at $Re_{\infty,L}$ from $0.3x10^6$ to $2.1x10^6$ for α between 0° and 50°. Angles of attack between 0° and 45° at a $Re_{\infty,L}$ of $0.2x10^6$ were obtained in the Mach 6 CF4 tunnel. All three facilities were used to acquire sideslip data, and aileron data was only acquired in the Mach 6 facilities.

Wind Tunnel Uncertainty Analysis

The accuracy of the experimental data was determined using the small sample method presented by Kline and McClintok[5]. In order to characterize and certify the balance, a strain gage calibration was performed prior to the tests and the full scale loads and associated uncertainties are summarized in Table III. Weight tares, sting deflections under load, and balance interactions were accounted for using standard procedures[6].

The small sample method for determining uncertainties described by Kline and McClintok helps to assess the significance of each uncertainty's contribution to the total, as well as to provide a more complete uncertainty evaluation (see Table IV). The largest sources of error in the present study are believed to be associated with the balance accuracy (see Table III), angle of attack and sideslip (±0.1°), reference moment center transfer distances (±0.002 in.), and freestream pitot pressure (±2%). As discussed in more detail by Brauckmann[7] et.al., the computed Mach number is directly affected by the accuracy of the free-stream pitot pressure measurement, as well as facility calibration measurements of spatial variation in the tunnel section. Therefore, since the Mach number computation is necessarily tied to the dynamic pressure, the free stream measurement and spatial variations directly affect reduction of the force data into coefficient form.

Computational Techniques

Computational Fluid Dynamics Solutions

Codes: The numerical tools used for this study include two computational fluid dynamics codes. The flowfield solver, IEC3D[1-2], has been extensively validated for

inviscid perfect gas and equilibrium air solutions based on the Shuttle Orbiter configuration. For inviscid solutions, IEC3D makes use of Van Leer's flux-vector splitting The fluxes are extended to higher order using the upwind total variation-diminishing (TVD) scheme of Osher and Chakravarthy. The solutions are obtained using a finite volume multi-block scheme together with an LU-SGS (Lower-Upper Symmetric Gauss-Seidel) implicit solver. Additional information about the application of IEC3D to the X-38 configuration can be found elsewhere[1]. The GASP[8] code has been applied to several geometries in order to obtain hypersonic aerodynamics. The GASP results from Reference 9 were obtained with Van Leer split flux with third order TVD limiting. The solutions were obtained using a finite volume multi-block scheme together with a two factor AF Relaxation algorithm. A real gas solution at a flight condition was obtained with a five species chemical non-equilibrium model (O_2, N_2, O, N, NO).

Geometry and Grids: The geometry of the X-38 is illustrated in Figure 1. The surface representation was created in the PRO ENGINEERING[10] solid modeling software and was transferred to the ICEMCFD[11] software package in order to construct an initial surface body grid. The ICEMCFD surface grid was then transferred to the GRIDGEN[12] structured grid generation package in order to refine the surface grid and add additional features such as the body elevon deflection. The volume grids were generated hyperbolically using the HYPGEN[13] program. The vehicle aerodynamic surfaces were set to 25° for the lower elevon and 10° outboard for the rudder built in as the zero reference setting. The wind tunnel grids have 165 streamwise points, 60 body to outer boundary points, and 130 points in the circumferential direction. An example of the final grid from a Mach 6 Air, α 40° CFD analysis is presented in Fig. 2. A similar topology was used for the flight condition solution with 165 streamwise points, 61 body to outer boundary points, and 185 points in the circumferential direction. The grid resolution for the flight case enabled a more appropriate modeling of the channel between the left and right elevons on the windward surface. To better approximate this channel, a constant coefficient of pressure was applied at the body surface to allow flow through in this region. The wind tunnel CFD simulations did not attempt to simulate the flow into the channel, i.e. the body surface was assumed to be solid in the channel region.

Results and Discussion

Wind Tunnel

Wind tunnel data from the three hypersonic facilities described previously encompassed the basic longitudinal and lateral-directional hypersonic characteristics of the X-38. Hypersonic trim will occur for elevon settings between 15° and 25°, so the focus of this discussion will be limited to 0° and 25° deflections. The longitudinal aerodynamic characteristics for 0° and 25° elevons are illustrated in Figure 3. Lift over drag curves plotted in Figure 4 for the three facilities illustrate only small differences above 30° α. Good agreement of the Mach 20 He and Mach 6 Air pitching moment is seen for 40° and 50° α, with a progressively larger pitch up increment illustrated for 20° and 30° α for both elevon settings. However, this effect is more pronounced for the 25° elevon setting. At the 0° elevon setting for the Mach 6 experiments, the CF4 data shows a positive increment in pitching moment at higher α which becomes slightly negative below 30° α. For the 25° elevon setting, the entire α range exhibits a negative pitching moment increment.

The shift in the CF4 data from a basically positive increment in pitch at 0° elevon, to a slightly negative increment for the 25° elevon would seem to be driven by effects in the elevon region. As illustrated by surface oil flows obtained in the Mach 6 Air facility (see Figure 5 and 6), a typical elevon separation bubble exists. This separation region has an effect on the elevon effectiveness and will be sensitive to the local flow conditions. The pitching moment

curves in Figure 3 illustrate elevon effectiveness for Mach 20 Helium which is quite consistent with the Mach 6 air effectiveness. However, the Mach 6 CF4 effectiveness is higher. The CF4 data demonstrates that the 25° elevon more than overcomes the positive pitch increment exhibited at high α with a 0° elevon. Based on the complete data set at high α, this crossover from a net positive to negative pitching moment increment occurs between 15° and 20° elevon settings .

By examining Schleiren images taken in the Mach 6 Air and CF4 facilities, more light can be shed on the elevon flowfield region effects on the pitching moment. Since the CF4 facility simulates the effect of a different density ratio across a shock, it is indicative of the high mach number and altitude effects on a reentry vehicle. The Mach 6 CF4 results demonstrate increased elevon effectiveness in comparison with the Mach 6 air data. The Schleiren images in Figures 7 and 8 correspond to runs at 40° α with a 25° elevon setting. Note the difference in shock standoff distance between the Mach 6 air and CF4 images. The standoff distances of both the bow shock and the elevon generated shock are smaller for the CF4 experiment, illustrating the effect of the different gamma. The effect on the longitudinal aerodynamics is due to increased pressure at the stagnation region, and increased pressure on the elevons. Because the elevon area is large compared to the stagnation region, when it is sufficiently deflected the net positive pitch increment for the 0° elevon depicted in the α sweeps of Figure 3 is negated.

Reynolds number dependency and lateral directional characteristics are presented in Figures 9-11. Mach 6 air pitching moment results in Figure 9 demonstrate a gradual decrease in pitching moment with increasing $Re_{\infty,L}$. This is most likely due to a slight change in the leeward separation line location and an effect on the elevon hinge line separation region.

The lateral and directional stability of the X-38 vehicle is crucial for its simplified design in that a cold gas reaction control system is desired to decrease complexity and reduce the risk due to hazardous materials, e.g.. propellants. Yawing moment and rolling moment data for -4° of yaw are presented in Figure 10 for all three facilities included in this study. Positive static directional stability, i.e. $C_{n\beta}$, is exhibited across the entire α range and adverse roll characteristics are evident. The severity of the adverse roll can only be understood by taking into account the aileron effectiveness. One measure of the lateral-directional stability is obtained by examining the effect of aileron upon the basic vehicle stability. When looking at this aspect of vehicle control, it is important to examine in a coupled fashion the yaw and roll derivatives due to sideslip and aileron. This can be accomplished by plotting the C_n versus C_l derivatives for sideslip and aileron, as in Figure 11. The upper left quadrant contains the sideslip derivatives of C_n and C_l, for 0° elevon deflections across the alpha range. The bottom right set of data corresponds to the aileron derivatives of C_n and C_l for 25° elevon and 10° aileron. What is undesirable is to have the slopes of the sideslip and aileron derivatives parallel. The data for the X-38 is fairly consistent across the angle of attack range and is sufficient in a generic sense. A complete lateral-directional stability assessment can only be done in unison with a flight control system. However, the hypersonic data shown in Fig. 11 is acceptable from a basic engineering standpoint.

Computational Fluid Dynamics Solutions

The use of Computational Fluid Dynamics (CFD) solutions for engineering understanding of hypersonic vehicle aerodynamics at flight conditions is well accepted, in large part because of Orbiter experience. In this frame of thought, a comparison with the Mach 6 air data helps to provide confidence that we can apply our CFD methodology to the flight environment. Results from the IEC3D code for viscous and inviscid longitudinal aerodynamics at Mach 6 air conditions are compared to the results

from the LaRC facility in Figures 12 and 13. The inviscid CFD results are seen to display consistent trends with the wind tunnel data, but are biased in magnitude. The importance of the separation region at the hinge line of the elevon as depicted in the oil flows discussed previously (see Figures 5-6), is thus demonstrated. As discussed in the Wind Tunnel Data section, the Mach 6 CF4 wind tunnel data demonstrated increased elevon effectiveness in comparison with the Mach 6 Air and Mach 20 He data. We can better understand how the wind tunnel results relate to the flight environment by comparing perfect gas and nonequilbirium chemistry solutions from GASP for a X-38 flight condition near Mach 22. As depicted in Figure 12, the constant gamma (1.4) solution at Mach 22 shows a more positive pitching moment than the nonequilibrium chemistry solution. This is consistent with the increased elevon effectiveness results obtained from the Mach 6 CF4 facility. The lift-to-drag ratio (Figure 13) for both the inviscid and viscous solutions at wind tunnel and flight conditions all agree reasonably well with the experimental data.

Summary

Wind tunnel data from the LaRC Mach 20 Helium, Mach 6 Air, and Mach 6 CF4 facilities have been compared for the X-38 configuration based on an X-23/X-24A derived vehicle. The hypersonic aerodynamics of this configuration do not appear to present any significant issues, as demonstrated by data taken in the facilities tested up to this time. Pitch trim is achievable within reasonable limits on elevon deflection. Mach number and high temperature effects demonstrate that elevon effectiveness increases when real gas effects are taken into account, either by testing in a heavy gas (CF4 tunnel) or through the application of CFD at flight conditions. Directional stability, as demonstrated by wind tunnel results, is maintained across the angle of attack range necessary for this vehicle's International Space Station support mission. Lateral-directional stability also appears to be acceptable. Comparison of the CFD results at wind tunnel conditions demonstrate acceptable differences in pitching moment and lift-to-drag ratio when the difference of elevon modelization is taken into account. Follow on hypersonic testing will involve entering higher Reynolds number facilities and increasing the fidelity of the elevons.

Conclusions

The X-38 Program is designing a vehicle that will be capable of returning six International Space Station crew members to earth when necessary. The hypersonic vehicle aerodynamics of the X-23/X-24A configuration demonstrates a robustness that betrays the amount of configuration tailoring involved in it's development in the 1960's. The hypersonic pitching moment characteristics are well behaved and are very understandable. The elevon effectiveness of the X-38 configuration increases with Mach number due to real gas effects, and is favorable from the standpoint of thermal constraints on the elevon design. Solutions provided with CFD at wind tunnel and flight conditions help to reinforce our understanding of the hypersonic aerodynamic characteristics. The lateral and directional stability is acceptable. However, more work will be necessary to understand the entire vehicle system design's capabilities in overcoming critical issues such as y-center of gravity offset impacts on hypersonic vehicle control.

Acknowledgements

The authors would like to thank Ethiraj Venkatapathy the ThermoSciences Institute and Mark Loomis and Carol Davies of and Sterling Software, all of NASA-Ames Research Center for providing the GASP viscous solution data for this paper.

References

1. Campbell, C.H., Caram, J., Li, C.P., and Madden, C., "Aerothermodynamic Environment Definition for an X-23/X-24A Derived Crew Return Vehicle,"

31st AIAA Thermophysics Conference, AIAA 96-1862, June, 1996.

2. Campbell, C.H., Joosten, B.K., and Meyerson, R.E., "Johnson Space Center Crew Return Vehicle Activities," SPACE 96 - Fifth ASCE International Conference on Engineering, Construction and Operations in Space, June, 1996.

3. Micol, J.R., "Hypersonic Aerodynamic/Aerothermodynamic Testing Capabilities at Langley Research Center: Aerothermodynamic Facilities Complex," AIAA 30th Thermophysics Conference, June 19-22, 1995, San Diego, CA, AIAA 95-2107.

4. Miller, C.G., "Langley Hypersonic Aerodynamic/Aerothermodynamic Testing Capabilities - Present and Future," AIAA 16th Aerodynamic Ground Testing Conference, June 18-209, 1995, Seattle, WA, AIAA 90-1376.

5. Kline, S., and McClintok, F., "Describing Uncertainties in Simple-Sample Experiments", Mechanical Engineering, pp. 3-8, 1953.

6. Keyes, J., "Force Testing Manual for the Langley 20-in. Mach 6 Tunnel", NASA TM-74026, 1977.

7. Brauckmann, G., Paulson, J., and Weilmuenster, K., "Experimental and Computational Analysis of Shuttle Orbiter Hypersonic Trim Anomaly", 1995, Journal of Spacecraft and Rockets, Vol. 32, No. 5.

8. GASP Version 3 User Manual, May, 1996.

9. Loomis, M.P., Venkatapathy, E., Papadapoulos, P., Davies, C.B., and Campbell, C.H., "Aerothermal CFD Validation and Prediction for the X-38 Program", Abstract Submitted to the AIAA 32nd Thermophysics Conference June 23-25, 1997.

10. ProEngineer, a product of Parametric Technology Corporation.

11. ICEM CFD/CAE MULCAD, version 3.1.3.0 Reference Manual, July, 1994.

12. Chawner, J.R., and Steinbrenner, J.P., "GRIDGEN Version 10 Training Course Notes," 1994.

13. Chan, W.M., Chiu, I.T., Buning, P.G., "User's Manual for the HYPGEN Hyperbolic Grid Generator", Sept. 1993.

Model	*Scale*	*Sref* [in2]	*b* [in]	*L* [in]	*Xref* [in]	*Zref* [in]
X-38 Flight	1.0	23,328	120	276	157.32	26.386
X-38 Tunnel	0.021	10.287	2.52	5.796	3.304	0.554

Table I. Reference Dimensions

Facility	*Test Gas*	M_∞	Re_∞, L (10^6)	$\rho_\infty/\rho 2$	$\gamma 2$	P_t [psia]	T_t [°F]
20" Mach 6	CF4	5.9	0.2	11.7	1.10	1050	750
20" Mach 6	Air	5.9	0.3	5.3	1.4	30	410
		5.9	0.6	5.3	1.4	60	425
		5.9	1.1	5.3	1.4	125	450
		5.9	1.5	5.3	1.4	180	450
		5.9	2.1	5.3	1.4	250	450
22" Mach 20	He	19.5	3.0	4.0	1.667	800	65

Table II. Representative Wind Tunnel Conditions

Balance	*Beam*	*Full Scale Load* [lb or in-lb]	*Accuracy % Full Scale* ($\pm 2\sigma$)
SSO9C	Normal	30	0.07
	Axial	8	0.09
	Pitch	30	0.08
	Roll	5	0.48
	Yaw	5	0.29
	Side	5	0.22

Table III. Balance Specifications and Accuracy

Tunnel	C_N	C_A	C_m	C_l	C_n	C_Y
Mach 20	±0.0217	±0.0020	±0.0014	±0.0012	±0.0009	±0.0031
Mach 6 CF4	±0.0214	±0.0055	±0.0015	±0.0014	±0.0007	±0.0023
Mach 6 Air $Re_{\infty,L}$ (10^6)						
0.3	±0.0265	0.0083	±0.0025	±0.0021	±0.0009	±0.0029
0.6	±0.0240	±0.0054	±0.0017	±0.0013	±0.0004	±0.0014
1.1	±0.0238	±0.0042	±0.0017	±0.0011	±0.0003	±0.0008
1.5	±0.0240	±0.0039	±0.0017	±0.0010	±0.0002	±0.0006
2.1	±0.0242	±0.0036	±0.0015	±0.0010	±0.0003	±0.0005

Table IV. Experimental Aerodynamic Coefficient Uncertainties

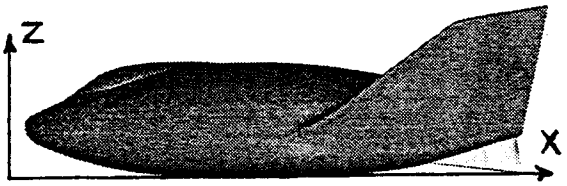

Figure 1. X-38 Geometry

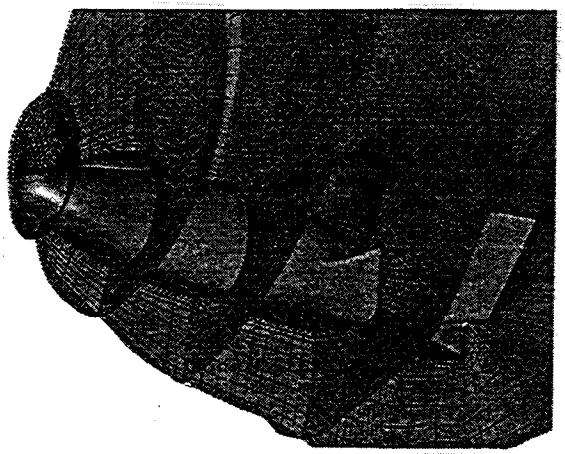

Figure 2. Mach 6 Air CFD Grid

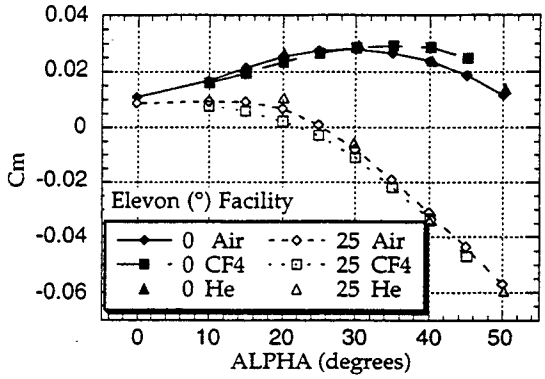

Figure 3. Experimental Hypersonic Pitching Moment

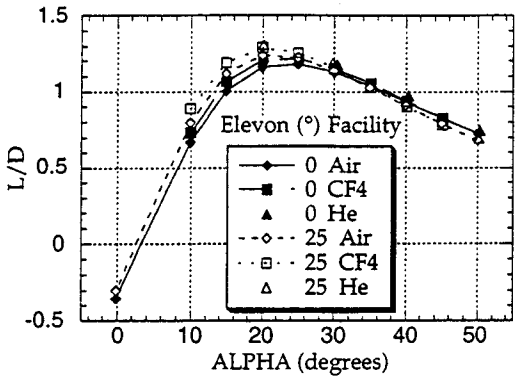

Figure 4. Experimental Hypersonic Lift to Drag Ratio

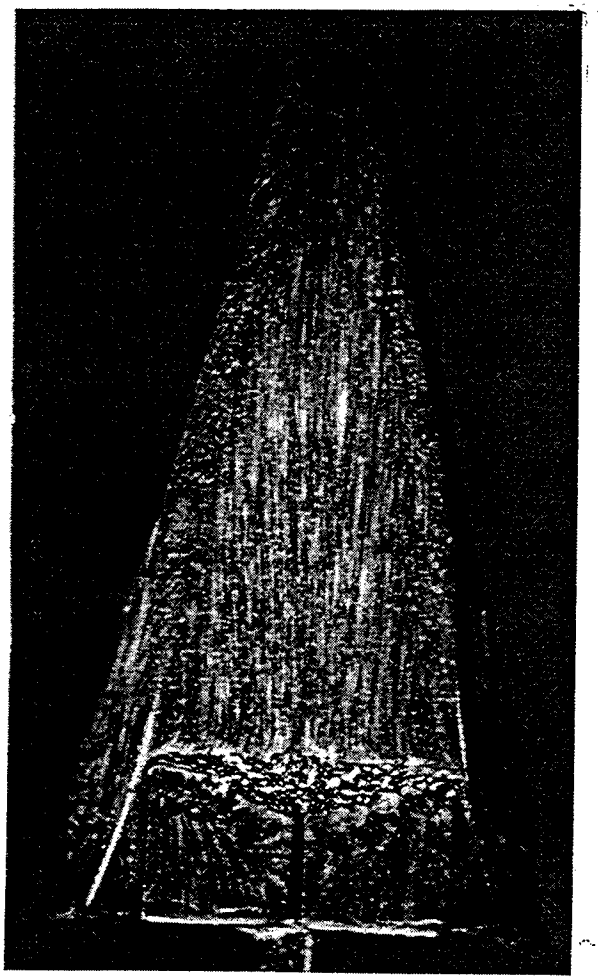

Figure 5. Mach 6 Air Surface Oil Flow for 20° Elevon, 20° Alpha

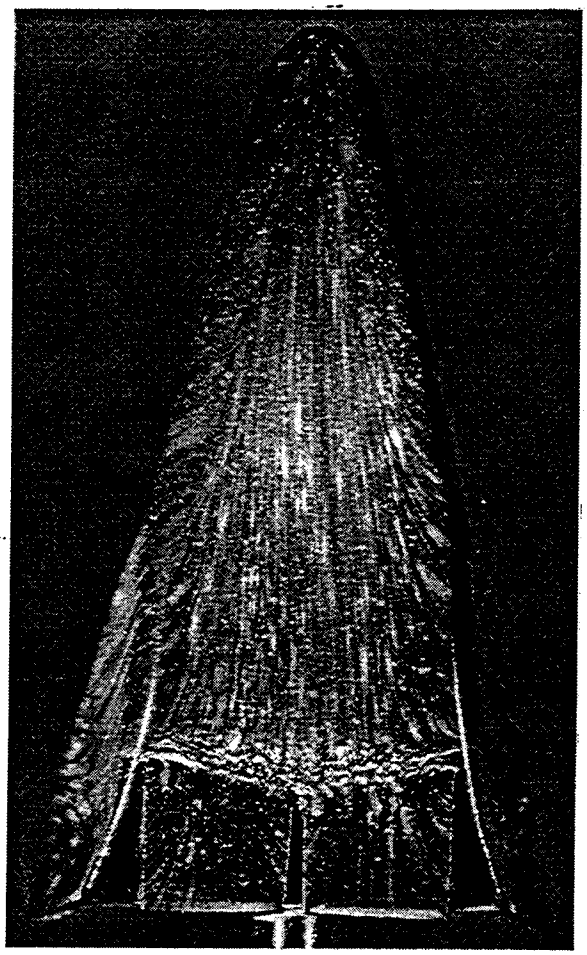

Figure 6. Mach 6 Air Surface Oil Flow for 20° Elevon, 40° Alpha

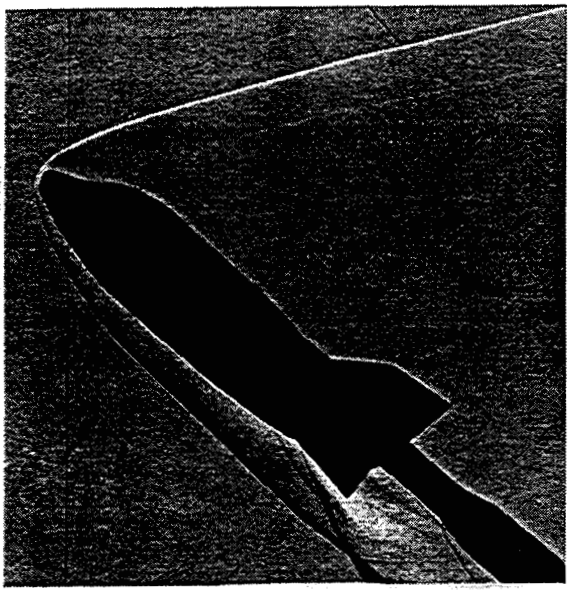

Figure 7. Mach 6 Air Schlieren Image for 25° Elevon, 40° Alpha

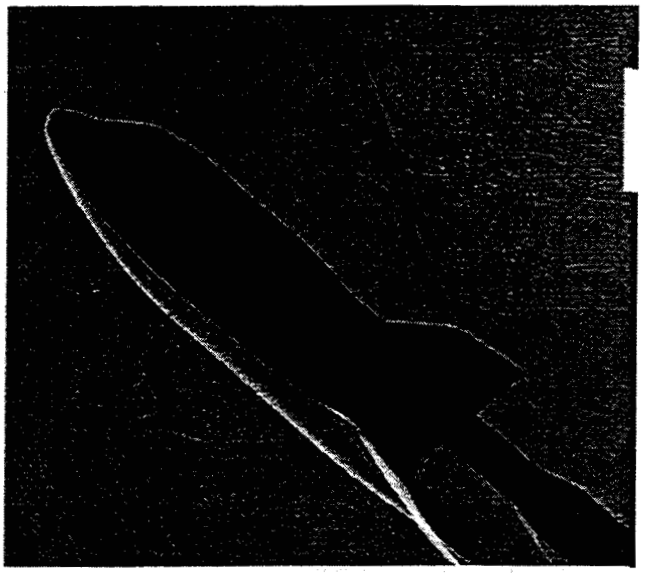

Figure 8. Mach 6 CF4 Schlieren Image for 25° Elevon, 40° Alpha

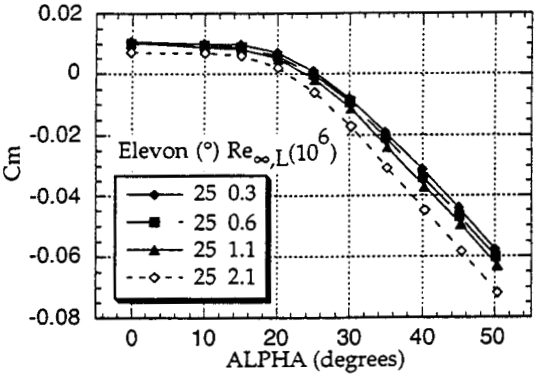

Figure 9. Experimental Hypersonic Pitching Moment $Re_{\infty,L}$ Effects for Mach 6 Air

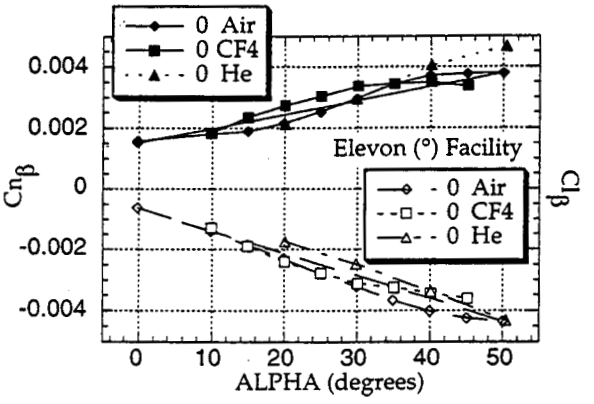

Figure 10. Experimental Hypersonic Directional Stability

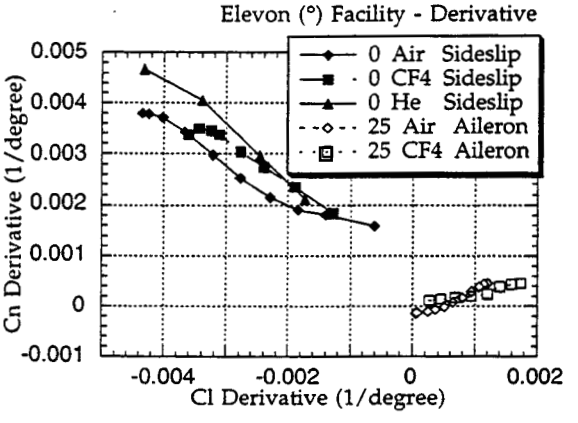

Figure 11. Experimental Hypersonic Lateral-Directional Stability

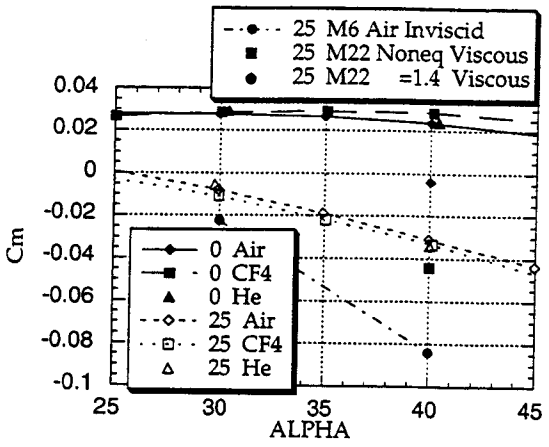

Figure 12. Comparison of Experimental and CFD Pitching Moment

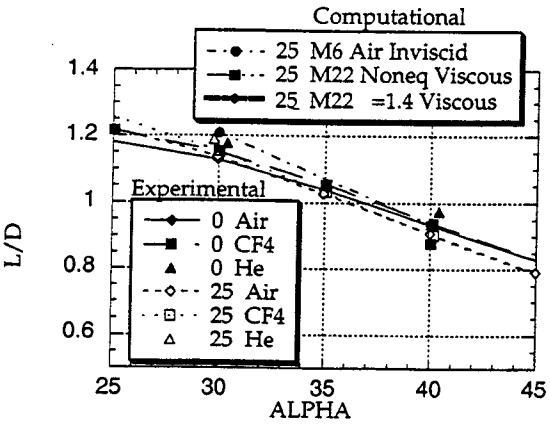

Figure 13. Comparison of Experimental and CFD Lift to Drag Ratio